

1 **Title: The impact of ischemic stroke on connectivity gradients**

2

3 **Authors:**

4 Şeyma Bayrak^{1,2}, Ahmed A. Khalil^{1,3,4}, Kersten Villringer³, Jochen B. Fiebach³, Arno
5 Villringer^{1,2,3,4}, Daniel S. Margulies⁵, Smadar Ovadia-Caro^{1,4,6}

6

7 **Affiliations:**

- 8 1. Department of Neurology, Max Planck Institute for Human Cognitive and Brain
9 Sciences, Leipzig, Germany
- 10 2. Department of Cognitive Neurology, University Hospital Leipzig and Faculty of
11 Medicine, University of Leipzig, Leipzig, Germany
- 12 3. Center for Stroke Research Berlin, Charité - Universitätsmedizin Berlin, Berlin,
13 Germany
- 14 4. Berlin School of Mind and Brain, Humboldt-Universität zu Berlin, Berlin,
15 Germany
- 16 5. Centre National de la Recherche Scientifique (CNRS) UMR 7225, Frontlab,
17 Institut du Cerveau et de la Moelle épinière, Paris, France
- 18 6. Department of Neurology, Campus Benjamin Franklin, Charité -
19 Universitätsmedizin Berlin, Berlin, Germany

20

21 **Correspondence:**

22 smadar.ovadia@gmail.com

23 Department of Neurology, Max-Planck Institute for Human Cognitive and Brain Sciences,
24 Stephanstrasse 1, 04103, Leipzig, Germany.

25

26 daniel.margulies@gmail.com

27 Institut du Cerveau et de la Moelle épinière
28 Hôpital Pitié-Salpêtrière
29 47, boulevard de l'Hôpital
30 75013 Paris, France

31

32 **Keywords:** connectivity gradients, intrinsic functional connectivity, diaschisis, resting-state
33 fMRI, connectome, diffusion embedding

34

35 **Abstract**

36 Understanding the relationship between localized anatomical damage, reorganization, and
37 functional deficits is a major challenge in stroke research. Previous work has shown that
38 localized lesions cause widespread functional connectivity alterations in structurally intact
39 areas, thereby affecting a whole network of interconnected regions. Recent advances suggest
40 an alternative to discrete functional networks by describing a connectivity space based on a
41 low-dimensional embedding of the full connectivity matrix. The dimensions of this space,
42 described as *connectivity gradients*, capture the similarity of areas' connections along a
43 continuous space. Here, we defined a three-dimensional connectivity space template based on
44 functional connectivity data from healthy controls. By projecting lesion locations into this
45 space, we demonstrate that ischemic strokes resulted in dimension-specific alterations in
46 functional connectivity over the first week after symptoms onset. Specifically, changes in
47 functional connectivity were captured along connectivity Gradients 1 and 3. The degree of
48 change in functional connectivity was determined by the distance from the lesion along these
49 connectivity gradients regardless of the anatomical distance from the lesion. Together, these
50 results provide a novel framework to study reorganization after stroke and suggest that, rather
51 than only impacting on anatomically proximate areas, the indirect effects of ischemic strokes
52 spread along the brain relative to the space defined by its connectivity.

53 **1.1 Introduction**

54

55 Stroke is defined as a sudden neurological deficit caused by a localized injury to the central
56 nervous system due to vascular pathology (Sacco et al., 2013). Outside of the localized
57 structural damage, areas connected to the lesion undergo functional alterations that are
58 implicated in symptomology and the recovery from neurological deficits. This phenomenon is
59 known as *diaschisis* (Andrews, 1991; Carrera and Tononi, 2014) and provides a theoretical and
60 empirical motivation to study brain connectivity following stroke.

61

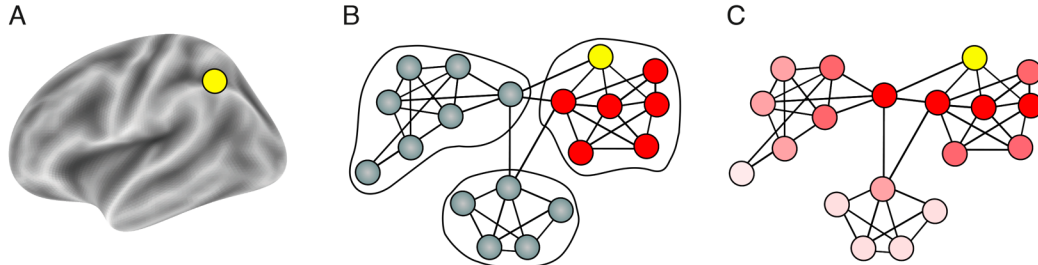
62 Functional connectivity based on the temporal correlation of ongoing blood-oxygen-level-
63 dependent (BOLD) fluctuations (resting-state functional magnetic resonance imaging; rs-
64 fMRI) has been successfully used to study alterations associated with reorganization within
65 functional networks. Previous studies found a reduction in functional connectivity after stroke
66 in structurally intact areas connected to the lesion (i.e., the affected network). Reduction in
67 functional connectivity was associated with the severity of the clinical deficit and recovery of
68 symptoms (Baldassarre et al., 2014; Carter et al., 2010; He et al., 2007; Ovadia-Caro et al.,
69 2013; Siegel et al., 2016; Wang et al., 2010; Warren et al., 2009). Importantly, normalization
70 of connectivity patterns was found following both spontaneous recovery (He et al., 2007; Park
71 et al., 2011; Ramsey et al., 2016; van Meer et al., 2010) and interventions using non-invasive
72 brain stimulation (Volz et al., 2016). Taken together, these findings support the phenomenon
73 of *diaschisis* and the view of stroke as a *network disruption* rather than a mere localized
74 phenomenon (Corbetta, 2010; Ovadia-Caro et al., 2014; Ward, 2005).

75

76 While previous studies demonstrate the role of the affected network in stroke pathology, the
77 impact of a lesion is not necessarily limited by network definitions. Graph models of brain
78 connectivity have demonstrated that the local disruption of a single node is likely to extend
79 beyond the affected network and impact, to varying degrees, the whole graph (Aerts et al., 2016;
80 Bassett and Bullmore, 2006; van den Heuvel and Sporns, 2013). Using predefined functional
81 networks assumes sharp boundaries between different functional domains. In addition, it
82 assumes that the effects of stroke are uniformly distributed within a given network. Contrary to
83 these assumptions, recent studies report that connectivity may be better captured by dimensions
84 representing the continuous space of the connectome (Atasoy et al., 2016; Cerliani et al., 2012;
85 Haak et al., 2018). With the shift in our understanding of cognitive brain functions as emerging
86 from global states (Bertolero et al., 2018; Cole et al., 2014; Sporns et al., 2005), so too our

87 models of brain dysfunction should attempt to characterize alterations at the whole-brain level,
88 taking the full connectome into account (see Figure 1).

89



90
91 **Figure 1. Two complementary views on brain organization and the corresponding**
92 **representation of distal effects of focal lesions.** (A) Representing a focal lesion (yellow node)
93 on the brain anatomical surface. (B) A schematic description of discrete networks parcellation
94 superimposed on a functional connectivity graph-space with nodes and edges. Using this
95 approach to study the effects of focal lesions (yellow node) restricts us to singular networks.
96 Additionally, distal effects of the lesion are assumed to be equally disruptive for all nodes in
97 the affected network (red nodes). (C) Representing functional connectivity in a continuous
98 manner without sharply defined borders using connectivity gradients. The lesioned node affects
99 all other nodes in the system as a function of the distance from the lesion in graph space (dark
100 red to light red). Using this approach does not assume sharp boundaries between functional
101 networks and provides a more realistic model of distant effects of localized lesions.

102

103
104 Recently, non-linear decomposition approaches have been introduced to represent whole-brain
105 rs-fMRI connectivity data in a continuous, low-dimensional space. This data-driven analysis
106 results in *connectivity gradients* that provide a low-dimensional description of the connectome
107 (Langs et al., 2016, 2014; Margulies et al., 2016). Each voxel is located along a connectivity
108 gradient according to its similarity of connections. Voxels that share a similar pattern of
109 functional connectivity are situated close to one another along a given connectivity gradient
110 (Huntenburg et al., 2018). Different functional modules are therefore clustered along a
111 continuum of a given connectivity gradient (Krienen and Sherwood, 2017) without the need of
112 a priori defined network parcellation.

113

114 Here, we studied the impact of localized lesions on continuous connectivity gradients.
115 Longitudinal rs-fMRI data were collected from patients following ischemic stroke. Data were
116 collected within 24 hours, as well as one and five days after the onset of stroke symptoms.
117 Changes in functional connectivity over the week were quantified using spatial concordance
118 (Lohmann et al., 2012). Data from healthy subjects were used to create a template of three
119 connectivity gradients representing all possible connections in a continuous manner.

120

121 Based on previous findings in discrete networks (Baldassarre et al., 2014; Carter et al., 2010;
122 He et al., 2007; Nomura et al., 2010; Ovadia-Caro et al., 2013; Siegel et al., 2016; Wang et al.,
123 2010; Warren et al., 2009) and computational models (Alstott et al., 2009; Honey and Sporns,
124 2008; van Dellen et al., 2013; Young et al., 2000), we hypothesized that a lesion along a
125 connectivity gradient would induce a gradual impact on the whole connectome. Functional
126 connectivity alterations would be most pronounced in areas that share a similar connectivity
127 pattern with the lesion.

128

129 **2.1 Materials and methods**

130

131 **2.2 Participants**

132

133 Fifty-four stroke patients (20 females, age: 63.78 ± 12.03 years, mean \pm SD) and 31 healthy
134 controls (13 females, age: 64.90 ± 8.49 years) were initially recruited for the study. Inclusion
135 criteria for patients were: patients older than 18 years, first ever ischemic stroke – small cortical
136 (≤ 1.5 cm) or subcortical, which was evident in imaging. A Wahlund score ≤ 10 (Wahlund et
137 al., 2001) to limit the extent of white matter lesions. Exclusion criteria included: clinical
138 evidence for antecedent lesions (n=3), fewer than 3 resting-state scans post-stroke (n=10),
139 lesions located solely within white matter (n=3 patients), corrupted MRI raw data or distorted
140 images (n=1 control, n=4 patients), high degree of head motion (n=1 control, n=6 patients), and
141 poor registration quality (n=1 control). For further details on quality assessment see
142 Supplementary Material M1.

143

144 Following the exclusion procedure, 28 stroke patients (11 females, age: 65.04 ± 13.27 years,
145 mean \pm SD), and 28 healthy controls (13 females, age: 65.21 ± 8.84 years) were included in
146 the analysis. The groups were matched for age and sex (age: Welch's t-test, P=0.95; sex:
147 Kruskal-Wallis H-test, P=0.59). For further details on patients' information see Supplementary
148 Table 1. The study was approved by the ethics committee of the Charité - Universitätsmedizin
149 Berlin, Germany (EA 1/200/13). Written informed consent was obtained from all participants.

150

151 **2.3 Neuroimaging data**

152

153 The MRI protocol included T1-weighted structural scans and T2*-weighted resting-state fMRI
154 scans (continuous fMRI scan with no overt task) for all participants. In addition, diffusion

155 weighted images (DWI; TR=8.2 s, TE=0.1 s, 50 volumes, voxel size: $2 \times 2 \times 2.5$ mm, flip angle
156 90°) and fluid attenuated inversion recovery images (FLAIR; TR=8.0 s, TE=0.1 s, 54 volumes,
157 voxel size: $0.5 \times 0.5 \times 5$ mm) were acquired from the stroke patients as part of a standard MRI
158 protocol (Hotter et al., 2009). All MRI data were acquired on a Siemens Tim Trio 3T scanner.
159 Healthy control participants were scanned at a single time point, whereas stroke patients were
160 scanned at three consecutive time points relative to stroke symptoms onset: day 0 (within 24
161 hours), day 1 (24 - 48 hours), and day 5 (range: day 4 – 6, mean 4.93 ± 0.38 SD). Structural
162 scans were acquired using a three-dimensional magnetization prepared rapid gradient-echo
163 (MPRAGE) sequence (TR=1.9 s, TE=2.52 s, TI=0.9 s, 192 slices, voxel size: $1 \times 1 \times 1$ mm, flip
164 angle 9°). Resting-state functional scans for each participant and session were acquired using
165 blood-oxygenation-level-dependent (BOLD) contrast with an EPI sequence (TR=2.3 s,
166 TE=0.03 s, 34 slices, 150 volumes, voxel size: $3 \times 3 \times 3$ mm, flip angle 90° , total duration=5.75
167 min).

168

169 **2.4 Data preprocessing**

170

171 T1-weighted structural images were preprocessed using FreeSurfer's recon-all pipeline (v6.0.0,
172 (Dale et al., 1999)). The pipeline generated segmentations for grey matter, white matter and
173 cerebrospinal fluid. Individual grey matter masks were registered to standard MNI space (3
174 mm^3).

175

176 Preprocessing of functional images included: *i*) removal of the first 5 EPI volumes to avoid
177 signal saturation, *ii*) slice timing and motion correction (Nipype v0.14.0, (Gorgolewski et al.,
178 2011; Roche, 2011)), *iii*) CompCor denoising approach for time series at the voxel level
179 (Nilearn v0.4.0, (Behzadi et al., 2007)), *iv*) temporal normalization, *v*) band-pass filtering in the
180 range of 0.01 - 0.1 Hz, and *vi*) spatial smoothing (applied after registration) with a 6 mm full-
181 width-half maximum Gaussian kernel using FSL (v5.0.9, (Woolrich et al., 2009)). Confounds
182 removed from the time series at the denoising step were defined as *i*) six head motion
183 parameters, including 1st and 2nd order derivatives, *ii*) motion and intensity outliers (Nipype's
184 rapidart algorithm; thresholds: $> 1\text{mm}$ framewise head displacement, and signal intensity > 3
185 SD of global brain signal accordingly) and *iii*) signal from white matter and cerebrospinal fluid.

186

187 The transformation of functional images to MNI152 (3 mm^3) space included a linear
188 transformation from EPI to the high-resolution T1-weighted image using FreeSurfer's

189 boundary-based register tool with 6 degrees of freedom (Greve and Fischl, 2009) and a
190 nonlinear transformation using ANTs (v2.1.0, (Avants et al., 2011)). The transformation
191 matrices obtained from both steps were concatenated and applied to the functional image using
192 a single interpolation.

193

194 **2.5 Lesion delineation**

195

196 Lesions were manually delineated by identifying areas of localized hyperintensity on day 0
197 DWI images using the ITK-SNAP software (v3.4.0, (Yushkevich et al., 2006)). Delineations
198 were guided by expert radiology reports and were approved by a radiology resident. All lesion
199 masks were normalized to MNI152 (3 mm³) space (ANTs, nearest-neighbor interpolation).
200 Individual lesion masks were smoothed in the atlas space using FSL's dilation tool with 3×3×3
201 kernel, extending the mask by one voxel-size (v5.0.9, (Jenkinson et al., 2012)).

202

203 **2.6 Computing connectivity gradients by applying nonlinear decomposition to functional 204 connectivity data from healthy controls**

205

206 To create a mutual grey matter template to be used for decomposition analysis, individual grey
207 matter masks and resting-state functional masks were averaged for all healthy controls to create
208 a group mask. Averaged group maps were multiplied to create a mutual mask such that only
209 grey matter voxels with fMRI signal would be included. The resulting template (33,327 voxels)
210 was used to generate functional connectivity matrices from individual healthy controls.

211

212 Functional connectivity matrices (33,327×33,327 voxels) were computed using Pearson's
213 correlation coefficient and were normalized using Fisher's z-transformation. An average
214 functional connectivity matrix was computed across healthy controls and the averaged z-scores
215 were transformed back to r-scores. Each row of the group-level functional connectivity matrix
216 was thresholded at 90% of its r-scores. This yielded an asymmetric, sparse matrix. The pairwise
217 cosine similarities of all rows were computed. By doing this, we obtained a non-negative and
218 symmetric similarity matrix, L (values in [0, 1] range).

219

220 We implemented the diffusion embedding approach on the similarity matrix to obtain a low-
221 dimensional representation of the whole-brain functional connectivity matrix (Coifman and
222 Lafon, 2006; Langs et al., 2016), as done in Margulies et al., 2016. This approach resulted in

223 gradients of functional connectivity. Voxels along each gradient are assigned unitless
224 embedding values. Along each gradient, voxels that share similar connectivity pattern have
225 similar embedding values.

226

227 **2.7 Mapping individual stroke lesions onto connectivity gradients from healthy controls**

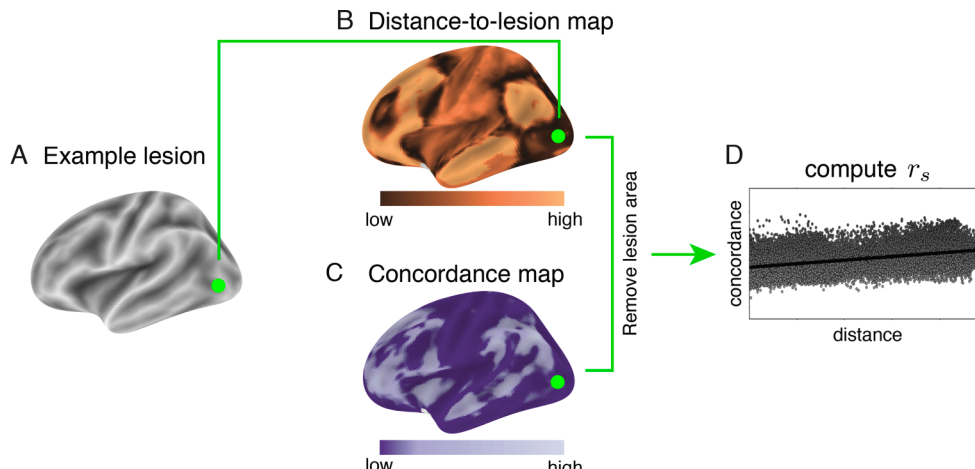
228

229 Individual lesion masks were projected onto the individual gradients obtained in healthy
230 controls. Lesioned voxels were marked according to their location along a specific gradient.
231 The lesion site along each gradient was defined as the minimum embedding value of all lesioned
232 voxels.

233

234 To quantify the functional similarity of non-lesioned voxels to the lesion site, distance-to-lesion
235 maps were computed for each non-lesioned voxel (Figure 2B). Distance values reflect the
236 mutual difference between embedding values of non-lesioned and lesioned voxels. Low
237 distance values reflect voxels that share similar functional connectivity pattern with the lesion
238 site.

239



240

241 **Figure 2. A schematic description of the analysis steps.** (A) Individual lesions were
242 delineated for each patient. Here, an example of a lesion located in the left occipital lobe
243 (green). (B) Distance-to-lesion maps were computed for each of the three connectivity
244 gradients. Distance values reflect the mutual difference between embedding values of non-
245 lesioned and lesioned voxels. Low distances (dark-copper) represent voxels that share a similar
246 functional connectivity pattern with the lesion site. This example shows the distance-to-lesion
247 map for the first gradient. (C) A voxel-wise spatial concordance map was computed for each
248 patient across the three resting-state scans after stroke. Concordance correlation coefficient
249 (CCC) values reflect the degree of change in the connectivity pattern over time for each voxel.
250 Low CCC values (dark-purple) represent voxels that underwent a larger change in their
251 functional connectivity pattern over time. (D) Spearman's rank correlation coefficient (r_s) was
252 used to test the relationship between distance-to-lesion and degree of functional connectivity
253 alteration across all voxels. A positive correlation depicts a larger change in functional

254 connectivity for voxels that were closer to the lesion site along the corresponding connectivity
255 gradient.

256

257 **2.8 Quantifying longitudinal alterations in functional connectivity matrices for stroke**
258 **patients**

259

260 For each patient, a functional mask was obtained from each of the three consecutive functional
261 scans. These masks were multiplied with the grey matter template of the healthy cohort. The
262 dilated lesion segmentations were then excluded from the patient-specific grey matter template.
263 This approach ensured that functional images of patients included only identical grey matter
264 voxels as healthy controls, except for the lesion site. The patient-specific grey matter templates
265 varied slightly in number of voxels included (ranging from 32,659 to 33,212 voxels).

266

267 To control for the slight variation in the number of voxels in patient-specific grey matter
268 templates, a control analysis was applied such that the grey matter template used for the analysis
269 contained 30,314 voxels in all patients prior to lesion removal. Using this more restricted mask
270 had no influence on our main results (see Supplementary Material M2 and Supplementary
271 Figure S1).

272

273 Functional connectivity matrices were computed using Pearson's correlation coefficient at each
274 of the three time points for individual patients. The voxel-wise spatial concordance map was
275 computed using the concordance correlation coefficient (CCC) (Lin, 2016) at the single-voxel
276 level across the three time points (Lohmann et al., 2012). CCC-values range between -1 and 1,
277 such that the lower concordance reflects larger alterations in the functional connectivity pattern
278 over time (Figure 2C).

279

280 **2.9 The relationship between lesion location along connectivity gradients and alterations**
281 **in functional connectivity after stroke**

282

283 Concordance correlation coefficient (CCC) values were correlated with distance-to-lesion
284 values using Spearman's rank-order correlation coefficient (Figure 2D). This analysis was
285 repeated for each connectivity gradient separately. Positive correlations suggest that changes in
286 functional connectivity are more pronounced in voxels that are close to the infarct region in the
287 corresponding gradient.

288 For a detailed description of the analysis steps see Supplementary Figure S2.

289 **2.10 The relationship between changes in functional connectivity over time and**
290 **anatomical lesion location**

291

292 Euclidean distances from each voxel to the infarct area in MNI152 (3 mm³) space using three-
293 dimensional voxel coordinates were computed for each patient. The resulting anatomical
294 distance values were correlated with concordance values (using Pearson's correlation
295 coefficient). A regression analysis was applied to remove the contribution of this factor from
296 CCC-values. Residuals were correlated with gradient-based distance-to-lesion values (using
297 Spearman's rank-order correlation coefficient).

298

299 **2.11 The relationship between changes in functional connectivity along connectivity**
300 **gradients and changes in clinical scores**

301

302 Individual gradients were divided into uniform parcels (bins). We varied the number of bins
303 used for the parcellation from 5 to 3000 in order to consider the continuous nature of
304 connectivity gradients while allowing us to classify parts of the gradients as affected by the
305 lesion. At each bin number and for each stroke patient, bins that overlapped with lesioned-
306 voxels were identified as “lesion-affected”, whereas the remaining bins were defined as “lesion-
307 unaffected”. An overall delta-concordance measure, ΔCCC , was computed as the difference
308 between average concordances in lesion-unaffected and lesion-affected bins, such that $\Delta CCC =$
309 $\mu_{unaffected} - \mu_{affected}$. A positive ΔCCC score reflects a higher functional connectivity
310 alteration over time in affected bins. Of note is that lesioned voxels were removed from this
311 computation, thereby the difference in concordance reflects the degree of preferential change
312 in functional connectivity in affected yet structurally intact areas.

313

314 To explore the link between changes in clinical scores and the overall delta-concordance
315 measure detected along gradients, the National Institute of Health Stroke Scale (NIHSS) was
316 used. The NIHSS values were assessed at the day of admission (day 0) and discharge (day 5).
317 Twenty-seven patients out of 28 completed the NIHSS assessment at both time points. Patients
318 were divided into two groups; those who changed in clinical score from day 0 to day 5 (“clinical
319 change”, n = 16), and those who did not change (“no clinical change”, n = 11).

320

321 Permutation test (with 10,000 iterations) was used to examine the significance of the difference
322 in mean ΔCCC values for the two groups of patients (“clinical change” versus “no clinical

323 change”). The test was repeated for each variation of bin numbers as well as for each of the
324 three connectivity gradients. Positive values reflect that a preferential change in concordance
325 over affected bins is more pronounced in patients who changed their clinical score from day 0
326 to day 5. To control for the multiple comparison problem resulting from varying the number of
327 bins ($N= 2996$ tests), the False Discovery Rate (FDR) correction (Benjamini and Hochberg,
328 1995) was applied with a threshold of 0.1.

329

330 **3.1 Results**

331

332 **3.2 Mapping stroke lesions onto connectivity gradients**

333

334 To map heterogeneous lesions across our sample of patients, individualized lesion masks were
335 delineated and projected onto a standard MNI brain (Figure 3A), as well as onto the first three
336 connectivity gradients (Figure 3B). Lesions were heterogeneous in both location and size (mean
337 volume= 4.11 cm^3 , SD= 2.80 cm^3), and distributed in subcortical ($n=13$), cortical ($n=14$), and
338 brainstem ($n=1$) regions. For further details on individual lesion location and affected vascular
339 territories, see Supplementary Table 1.

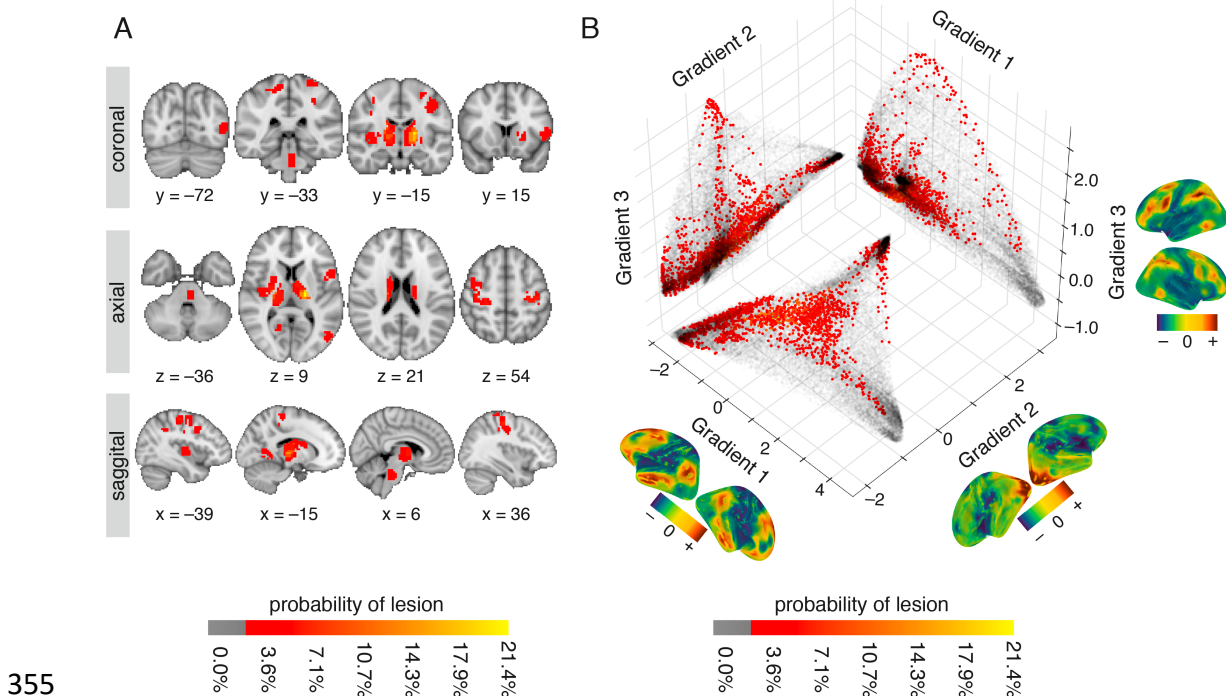
340

341 Projecting lesion locations onto the connectivity gradients enabled us to assess which portions
342 of connectivity space were affected by the stroke. The template connectivity space was based
343 on a decomposition of voxelwise functional connectivity data from healthy controls. Voxels
344 that share functional connectivity patterns are situated closer to one another along a given
345 connectivity gradient. For example, voxels that are part of the default-mode network are
346 clustered at the high end of Gradient 1, and those that are part of primary sensory areas at the
347 low end (Margulies et al., 2016). Here, we used the first three gradients that account for a total
348 variance of 50.84% in the healthy control connectivity data (see Supplementary Figure S3).

349

350 Figure 3B demonstrates the distribution of lesioned voxels within the three-dimensional
351 connectivity space. We found that although the anatomical location of lesions was
352 heterogeneous (Figure 3A), within the connectivity space lesions were predominantly clustered
353 at the extremes of each gradient, especially those of Gradients 1 and 3 (Figure 3B).

354



355
356

Figure 3. Lesion location across patients shown in anatomical space and along connectivity gradients (A) Anatomical lesion distribution in individual stroke patients (n=28) projected onto an MNI brain. The red-to-yellow color bar indicates the percentage of patients with lesions in that voxel. (B) Location of lesions projected onto the first three connectivity gradients. The three connectivity gradients represent a low-dimensional description of the whole-brain connectivity matrix obtained using healthy controls' data (n=28). Corresponding spatial maps of each connectivity gradient are projected on brain surface mesh near respective axes. Colors represent positive (sienna) and negative (dark blue) embedding values, in accordance with values along the axes. Along each gradient, voxels that share similar connectivity patterns are situated close to one another and have similar embedding values. Grey scatter plots depict a two-dimensional connectivity space created as a combination of any two given gradients. Lesion location along each gradient is projected onto the two-dimensional space as an alternative approach to anatomical lesion mapping. The red-to-yellow color bars indicates the percentage of patients with lesions in that voxel. Lesioned voxels are mostly clustered around the edges of the connectivity gradients such that they affect sensorimotor areas and ventral and dorsal areas associated with attention.

373
374

375 **3.3 The impact of lesion location along specific connectivity gradients on reorganization**

376

377 To determine if the location of lesions along specific gradients is associated with changes in
378 functional connectivity after stroke, we computed for each voxel: 1) spatial concordance, which
379 reflected the degree of change in the functional connectivity pattern over time. Spatial
380 concordance values range between -1 and 1 such that lower values reflect a larger change in
381 functional connectivity pattern over time; and, 2) distance-to-lesion along each connectivity
382 gradient. Distance values represent the similarity of functional connectivity patterns for any

383 given voxel with the lesioned area. Low distance values reflect voxels that share similar
384 functional connectivity pattern with the lesion site. Importantly, the lesioned voxels were
385 excluded from both these analyses such that only the indirect effects of the lesion (i.e.,
386 diaschisis) were assessed. Spatial concordance and distance-to-lesion were correlated for
387 individual patients, and individual connectivity gradients.

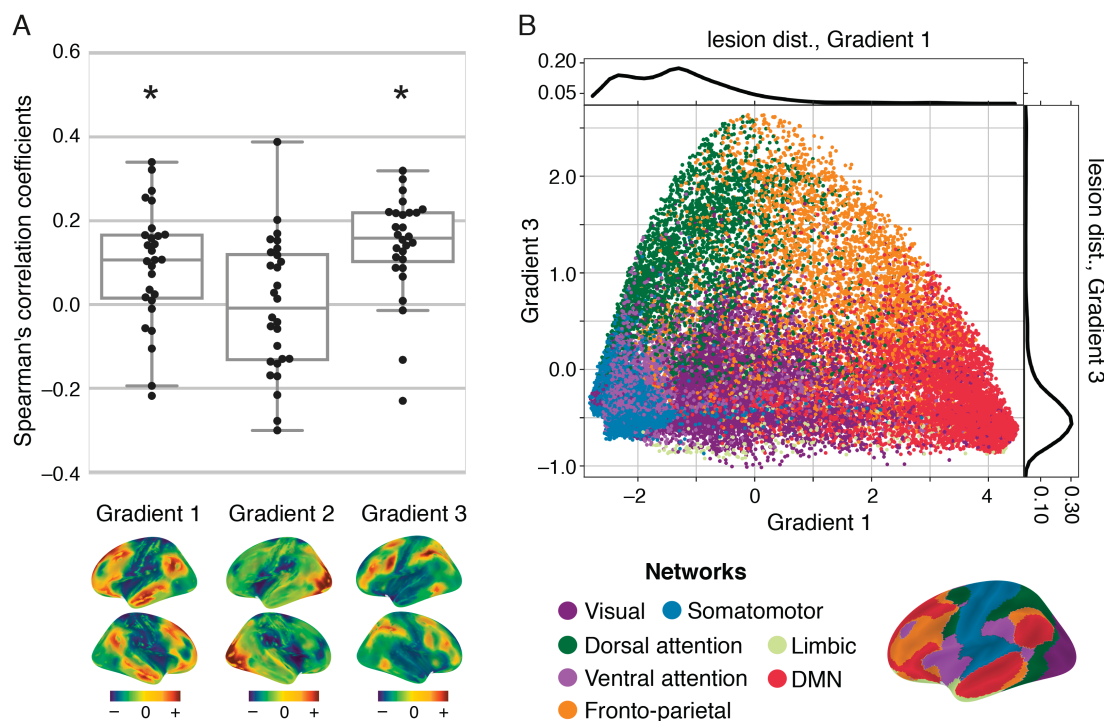
388

389 We found a significant relationship between the degree of functional connectivity alterations
390 over time and proximity of non-lesioned voxels to lesion locations along Gradient 1 and
391 Gradient 3. No significant relationship was found for Gradient 2 (Figure 4A, Table 1).

392

393 Figure 4B demonstrates the correspondence between the connectivity space described by
394 Gradients 1 and 3, and a canonical set of seven resting-state networks (Yeo et al, 2011).
395 Gradient 1 captures the dissociation between the default-mode network (DMN) and the
396 sensorimotor/visual networks, while Gradient 3 captures the dissociation between dorsal
397 attention/fronto-parietal networks and sensorimotor/visual/DMN networks. For a descriptive
398 analysis of the relationship between connectivity gradients and cognitive functions see
399 Supplementary Material M3 and Supplementary Figure S4.

400



401

402 **Figure 4. The relationship between lesion location along connectivity gradients and the**
403 **degree of changes in functional connectivity in non-lesioned voxels over time. (A)**
404 **Correlation values between distance-to-lesion and spatial concordance (y-axis) are shown for**
405 **individual patients and the three connectivity gradients (x-axis). The spatial map of each**

406 connectivity gradient is shown below the respective location on the x-axis. Correlations were
407 significantly positive for Gradient 1 ($P=0.0027$, $W=71.0$, one-tailed Wilcoxon signed-rank test)
408 and Gradient 3 ($P=0.0001$, $W=35.0$), but not for Gradient 2 ($P=0.76$, $W=189.0$). The closer a
409 voxel is to the lesioned site mapped on connectivity gradients 1 and 3, the more pronounced its
410 functional connectivity changes over time. (B) Continuous connectivity gradients and
411 corresponding seven canonical resting-state networks (Thomas Yeo et al., 2011). Voxels are
412 situated based on their embedding values along Gradient 1 (x-axis) and 3 (y-axis) and colored
413 according to their network assignment. Gradient 1 captures the dissociation between the
414 default-mode network (DMN) and the sensorimotor networks on its two edges, while Gradient
415 3 captures the dissociation between dorsal attention/fronto-parietal networks and
416 sensorimotor/DMN networks on its two edges. Lesion distributions along connectivity
417 gradients are overlaid on the individual gradient axes. Lesions overlap most frequently with the
418 lowest ends of Gradients 1 and 3.
419

	Gradient 1	Gradient 2	Gradient 3
r-values	[-0.22, 0.34]	[-0.30, 0.39]	[-0.23, 0.32]
median	0.11	-0.01	0.16
W	71.00	189.00	35.00
p-values	0.0027*	0.76	0.0001*

420
421 **Table 1: summary of statistical results**
422 W; Wilcoxon signed-rank test.
423

424 Given the expected partial correlation between distance from the lesion in connectivity space
425 and anatomical distance, we further assessed whether anatomical location contributed to the
426 relationship with connectivity space. We found a significant relationship between distance from
427 the lesion in anatomical space and changes in functional connectivity over time ($P = 0.0042$,
428 one-tailed Wilcoxon signed-rank test). However, using anatomical distance as a regressor of no
429 interest did not alter the significance of our main result (see Supplementary Figure S5).
430 Functional connectivity therefore preferentially changes after stroke in voxels that are proximal
431 to the lesion location along Gradients 1 and 3. This relationship cannot be solely explained by
432 the anatomical distance from the lesion.
433

434 **3.4 Clinical relevance of functional connectivity alterations detected along connectivity 435 gradients**

436

437 Previous studies have linked alterations in functional connectivity with clinical trajectory (He
438 et al., 2007; Ovadia-Caro et al., 2013; Park et al., 2011; Ramsey et al., 2016; van Meer et al.,
439 2010), thereby supporting the functional significance of connectivity changes after stroke. We
440 thus explored the relationship between functional connectivity changes and patients' clinical
441 trajectory for each connectivity gradient.
442

443 We tested for a group difference in spatial concordance in affected yet structurally intact areas
444 between patients who demonstrated a change in clinical scores from day 0 to day 5 and those
445 who did not. A positive difference in the mean of the two groups reflects an association between
446 preferential changes in functional connectivity in affected areas and a change in clinical scores
447 over the first week after stroke. To maintain the continuous nature of connectivity gradients,
448 we varied the number of bins used to divide the gradients into parcels of equal size (bin numbers
449 ranged from 5 to 3000). We found no significant difference between patients who changed in
450 clinical scores and those who did not for any of the connectivity gradients, across different bin
451 numbers. The averaged difference in mean for the two groups was 0.0014 (range: -0.004 to
452 0.015) for Gradient 1, 0.0095 (range: 0.003 to 0.015) for Gradient 2, and 0.011 (range: 0.0012
453 – 0.019) for Gradient 3. The range of corresponding p-values was 0.15 to 0.61 for Gradient 1,
454 0.12 to 0.4 for Gradient 2, and 0.03 to 0.46 for Gradient 3 (see Supplementary Figure S6).

455

456 **4.1 Discussion:**

457

458 We found that stroke induces a gradual change in functional connectivity along specific
459 connectivity gradients. Beginning with data acquired on the day of symptom onset, we showed
460 that the degree of reorganization over the first week is influenced by the lesion location along
461 connectivity Gradients 1 and 3. Voxels that are close to the lesion within this connectivity space
462 demonstrate a preferential change in functional connectivity over time, regardless of their
463 anatomical distance from the lesion.

464

465 We have implemented a decomposition approach that overcomes the necessity to parcellate the
466 brain into discrete networks, retains information from single voxels and provides a data-driven
467 template for studying reorganization at the connectome-level. We therefore show that strokes
468 result in widespread connectivity changes that progress gradually along the connectome.

469

470 Our results are in line with previous studies that have used a priori defined networks. Functional
471 connectivity alterations after stroke have been reported for sensorimotor, language and attention
472 networks (Baldassarre et al., 2014; Carter et al., 2010; He et al., 2007; Ovadia-Caro et al., 2013;
473 Siegel et al., 2016; Wang et al., 2010; Warren et al., 2009). These previous studies support the
474 notion that localized lesions induce widespread effects in structurally intact areas connected to
475 the lesion, creating a *diaschisis* effect (Andrews, 1991; Carrera and Tononi, 2014). Stroke is
476 therefore not a strictly localized pathology (Corbetta, 2010; Ovadia-Caro et al., 2014; Ward,

477 2005). Remote, structurally intact areas undergo functional changes as part of the
478 reorganization process.

479

480 Here, we extend these findings to the continuous representation of the connectome. We
481 demonstrate that reorganization, as reflected in functional connectivity alterations, changes as
482 a function of the distance along specific connectivity gradients. However, it is not exclusively
483 restricted to the affected network. Thus, while most pronounced changes take place in
484 connected areas, the effects of stroke gradually spread along the connectome.

485

486 We found that connectivity Gradients 1 and 3 better predicted the impact of a lesion on
487 functional connectivity than Gradient 2. The three connectivity gradients capture distinct
488 connectivity axes, with different functional domains on their extremes. One crucial difference
489 between these gradients is that Gradient 2, in contrast to the others, represents a spectrum of
490 relatively local patterns of connectivity (Felleman and Van Essen, n.d.; Markov et al., 2014),
491 spanning sensory and motor systems. Regions emphasized in Gradient 2 are less likely to
492 demonstrate changes following localized lesions, as there is little redundancy owing to long-
493 distance connectivity. However, it remains to be investigated if changes in functional
494 connectivity can be captured along Gradient 2 using a more homogenous lesion sample
495 impacting only the far extremes of this gradient.

496

497 Our study demonstrates the importance of the lesion location within connectivity space for
498 understanding the reorganization of functional connectivity. However, distance from the lesion
499 in connectivity space is partially related to the anatomical distance, as areas close to one another
500 often have similar connectivity patterns. In addition, local physiological changes in areas
501 directly surrounding the lesion (Dirnagl et al., 1999) can also contribute to changes in functional
502 connectivity (Khalil et al., 2017; Siegel et al., 2016). We therefore calculated in a control
503 analysis the Euclidian distances from each voxel to the infarct area using a three-dimensional
504 anatomical space. We found a significant relationship between distance based on anatomy and
505 changes in functional connectivity as measured by spatial concordance. However, when
506 regressing out the contribution of this factor from our main analysis, the results did not change
507 (see Supplementary Figure S5). Consequently, changes in functional connectivity detected
508 along connectivity gradients could not be solely explained by lesion topography or
509 physiological processes occurring in the vicinity of the lesion site. In addition, this analysis

510 emphasizes the significant contribution of functional connectivity changes in distant areas to
511 the global process of reorganization.

512

513 The link between changes in functional connectivity after stroke, clinical deficits and clinical
514 recovery has been previously shown (He et al., 2007; Ovadia-Caro et al., 2013; Park et al.,
515 2011; Ramsey et al., 2016; van Meer et al., 2010). Here, we applied an exploratory analysis of
516 the relationship between lesion location along connectivity gradients, changes in functional
517 connectivity, and changes in clinical scores (NIHSS) over the first week. We divided the
518 patients into two groups according to whether or not a clinical change took place over the first
519 week.

520

521 Given previous findings, we expected a significant difference between the groups in the degree
522 of change in functional connectivity patterns, however, we found no such difference for any of
523 the connectivity gradients. Of interest nevertheless is that for Gradient 2 and Gradient 3, group
524 differences were not randomly distributed and were positive in values (see Supplementary
525 Figure S6).

526

527 The lack of a relationship between changes in functional connectivity and changes in clinical
528 scores could be explained by the usage of NIHSS. NIHSS is the most commonly used
529 assessment scale in routine acute stroke management. However, this score is fairly coarse and
530 is not designed to accurately detect individual neurological deficits. It is instead intended to
531 provide a standardized and reproducible overall assessment of how stroke affects a patient's
532 neurological status (Lyden, 2017). The relationship between functional connectivity changes
533 along specific connectivity gradients and stroke symptomology assessed using a more detailed
534 clinical assessment (which would better fit the voxelwise information retained in the gradients,
535 particularly for parcellations that contain a small number of voxels) remains to be investigated
536 in a larger sample of patients.

537

538 The conceptual shift from mapping brain regions to networks has provided a substantial
539 improvement in how we understand the organization of functional systems. Here we aimed to
540 translate the recent descriptions of a low-dimensional connectivity space to the clinical question
541 of stroke-induced damage. While future studies will be necessary to better understand the utility
542 of this framework for stroke prognosis, the current findings provide support for conceptualizing
543 brain connectivity within a continuous connectivity-defined space. Brain networks describe

544 interconnected regions, but similar to the problem of lesion delineation, they also require the
545 delineation of discrete boundaries. Connectivity space offers an advance by representing the
546 continuous nature of brain networks, but also by capturing their relative similarity. Further work
547 is necessary to develop a mode of describing this space in a cognitive and clinical neuroscience
548 context. Nevertheless, the current findings demonstrate its utility for capturing the impact of
549 localized damage to the space.

550

551 **5.1 Conclusions**

552

553 Studying changes in functional connectivity after stroke in a longitudinal manner provides
554 insight into the process of reorganization during the recovery of function. Connectivity
555 gradients represent a methodological advancement in how we depict functionally meaningful
556 information in the connectome. Using this fine-grained template that considers all connections
557 has the potential of informing more targeted stroke therapies that have yet to translate to clinical
558 usage, mostly due to oversimplified models of brain reorganization (Di Pino et al., 2014).

559

560

561 **Acknowledgements:**

562 The authors would like to thank the patients for participating in the study, and to Dr. Julia
563 Huntenburg, Dr. Luke Tudge and Sabine Oligschläger for their advice in various stages of this
564 project.

565

566

567

568

- 569 **References:**
- 570 Aerts, H., Fias, W., Caeyenberghs, K., Marinazzo, D., 2016. Brain networks under attack:
571 Robustness properties and the impact of lesions. *Brain* 139, 3063–3083.
572 <https://doi.org/10.1093/brain/aww194>
- 573 Alstott, J., Breakspear, M., Hagmann, P., Cammoun, L., Sporns, O., 2009. Modeling the
574 impact of lesions in the human brain. *PLoS Comput. Biol.* 5, e1000408.
575 <https://doi.org/10.1371/journal.pcbi.1000408>
- 576 Andrews, R.J., 1991. Transhemispheric diaschisis. A review and comment. *Stroke* 22, 943–
577 949. <https://doi.org/10.1161/01.STR.22.7.943>
- 578 Atasoy, S., Donnelly, I., Pearson, J., 2016. Human brain networks function in connectome-
579 specific harmonic waves. *Nat. Commun.* 7, 1–10. <https://doi.org/10.1038/ncomms10340>
- 580 Avants, B.B., Tustison, N.J., Song, G., Cook, P.A., Klein, A., Gee, J.C., 2011. A reproducible
581 evaluation of ANTs similarity metric performance in brain image registration.
582 *Neuroimage* 54, 2033–2044. <https://doi.org/10.1016/j.neuroimage.2010.09.025>
- 583 Baldassarre, A., Ramsey, L., Hacker, C.L., Callejas, A., Astafiev, S. V., Metcalf, N. V., Zinn,
584 K., Rengachary, J., Snyder, A.Z., Carter, A.R., Shulman, G.L., Corbetta, M., 2014.
585 Large-scale changes in network interactions as a physiological signature of spatial
586 neglect. *Brain* 137, 3267–3283. <https://doi.org/10.1093/brain/awu297>
- 587 Bassett, D.S., Bullmore, E., 2006. Small-World Brain Networks. *Neurosci.* 12, 512–523.
588 <https://doi.org/10.1177/1073858406293182>
- 589 Behzadi, Y., Restom, K., Liau, J., Liu, T.T., 2007. A component based noise correction
590 method (CompCor) for BOLD and perfusion based fMRI. *Neuroimage* 37, 90–101.
591 <https://doi.org/10.1016/j.neuroimage.2007.04.042>
- 592 Benjamini, Y., Hochberg, Y., 1995. Controlling the False Discovery Rate: a Practical and
593 Powerful Approach to Multiple Testing. *J. R. Stat. Soc.* 57, 289–300.
594 <https://doi.org/10.2307/2346101>
- 595 Bertolero, M.A., Yeo, B.T.T., Bassett, D.S., Esposito, M.D., 2018. A mechanistic model of
596 connector hubs, modularity, and cognition. *arXiv* 1–37. <https://doi.org/10.1038/s41562-018-0420-6>
- 598 Carrera, E., Tononi, G., 2014. Diaschisis: past, present, future. *Brain* 137, 2408–22.
599 <https://doi.org/10.1093/brain/awu101>
- 600 Carter, A.R., Astafiev, S. V, Lang, C.E., Connor, L.T., Rengachary, J., Strube, M.J., Pope,
601 D.L.W., Shulman, G.L., Corbetta, M., 2010. Resting interhemispheric functional
602 magnetic resonance imaging connectivity predicts performance after stroke. *Ann.*

- 603 Neurol. 67, 365–75. <https://doi.org/10.1002/ana.21905>
- 604 Cerliani, L., Thomas, R.M., Jbabdi, S., Siero, J.C.W., Nanetti, L., Crippa, A., Gazzola, V.,
605 D’Arceuil, H., Keysers, C., 2012. Probabilistic tractography recovers a rostrocaudal
606 trajectory of connectivity variability in the human insular cortex. Hum. Brain Mapp. 33,
607 2005–2034. <https://doi.org/10.1002/hbm.21338>
- 608 Coifman, R.R., Lafon, S., 2006. Diffusion maps. Appl. Comput. Harmon. Anal. 21, 5–30.
609 <https://doi.org/10.1016/j.acha.2006.04.006>
- 610 Cole, M.W., Bassett, D.S., Power, J.D., Braver, T.S., Petersen, S.E., 2014. Intrinsic and task-
611 evoked network architectures of the human brain. Neuron 83, 238–251.
612 <https://doi.org/10.1016/j.neuron.2014.05.014>
- 613 Corbetta, M., 2010. Functional connectivity and neurological recovery. Dev. Psychobiol. 54,
614 239–53. <https://doi.org/10.1002/dev.20507>
- 615 Dale, A.M., Fischl, B., Sereno, M.I., 1999. Cortical Surface-Based Analysis. Neuroimage 9,
616 179–194. <https://doi.org/10.1006/nimg.1998.0395>
- 617 Di Pino, G., Pellegrino, G., Assenza, G., Capone, F., Ferreri, F., Formica, D., Ranieri, F.,
618 Tombini, M., Ziemann, U., Rothwell, J.C., Di Lazzaro, V., 2014. Modulation of brain
619 plasticity in stroke: a novel model for neurorehabilitation. Nat. Rev. Neurol. 10, 597–
620 608. <https://doi.org/10.1038/nrneurol.2014.162>
- 621 Dirnagl, U., Iadecola, C., Moskowitz, M.A., 1999. Pathobiology of ischaemic stroke : an
622 integrated view 391–397.
- 623 Felleman, D.J., Van Essen, D.C., n.d. Distributed hierarchical processing in the primate
624 cerebral cortex. Cereb. Cortex 1, 1–47.
- 625 Gorgolewski, K., Burns, C.D., Madison, C., Clark, D., Halchenko, Y.O., Waskom, M.L.,
626 Ghosh, S.S., 2011. Nipype: A Flexible, Lightweight and Extensible Neuroimaging Data
627 Processing Framework in Python. Front. Neuroinform. 5.
628 <https://doi.org/10.3389/fninf.2011.00013>
- 629 Greve, D.N., Fischl, B., 2009. Accurate and robust brain image alignment using boundary-
630 based registration. Neuroimage 48, 63–72.
631 <https://doi.org/10.1016/j.neuroimage.2009.06.060>
- 632 Haak, K. V., Marquand, A.F., Beckmann, C.F., 2018. Connectopic mapping with resting-state
633 fMRI. Neuroimage 170, 83–94. <https://doi.org/10.1016/j.neuroimage.2017.06.075>
- 634 He, B.J., Snyder, A.Z., Vincent, J.L., Epstein, A., Shulman, G.L., Corbetta, M., 2007.
635 Breakdown of functional connectivity in frontoparietal networks underlies behavioral
636 deficits in spatial neglect. Neuron 53, 905–18.

- 637 <https://doi.org/10.1016/j.neuron.2007.02.013>
- 638 Honey, C.J., Sporns, O., 2008. Dynamical consequences of lesions in cortical networks. *Hum.*
639 *Brain Mapp.* 29, 802–9. <https://doi.org/10.1002/hbm.20579>
- 640 Hotter, B., Pittl, S., Ebinger, M., Oepen, G., Jegzentes, K., Kudo, K., Rozanski, M., Schmidt,
641 W.U., Brunecker, P., Xu, C., Martus, P., Endres, M., Jungehülsing, G.J., Villringer, A.,
642 Fiebach, J.B., 2009. Prospective study on the mismatch concept in acute stroke patients
643 within the first 24 h after symptom onset - 1000Plus study. *BMC Neurol.* 9, 1–8.
644 <https://doi.org/10.1186/1471-2377-9-60>
- 645 Huntenburg, J.M., Bazin, P.L., Margulies, D.S., 2018. Large-Scale Gradients in Human
646 Cortical Organization. *Trends Cogn. Sci.* 22, 21–31.
647 <https://doi.org/10.1016/j.tics.2017.11.002>
- 648 Jenkinson, M., Beckmann, C.F., Behrens, T.E.J., Woolrich, M.W., Smith, S.M., 2012. *Fsl.*
649 *Neuroimage* 62, 782–790. <https://doi.org/10.1016/j.neuroimage.2011.09.015>
- 650 Khalil, A.A., Ostwaldt, A.C., Nierhaus, T., Ganeshan, R., Audebert, H.J., Villringer, K.,
651 Villringer, A., Fiebach, J.B., 2017. Relationship between Changes in the Temporal
652 Dynamics of the Blood-Oxygen-Level-Dependent Signal and Hypoperfusion in Acute
653 Ischemic Stroke. *Stroke* 48, 925–931.
654 <https://doi.org/10.1161/STROKEAHA.116.015566>
- 655 Krienen, F.M., Sherwood, C.C., 2017. Gradients of Connectivity in the Cerebral Cortex.
656 *Trends Cogn. Sci.* 21, 61–63. <https://doi.org/10.1016/j.tics.2016.12.002>
- 657 Langs, G., Sweet, A., Lashkari, D., Tie, Y., Rigolo, L., Golby, A.J., Golland, P., 2014.
658 Decoupling function and anatomy in atlases of functional connectivity patterns:
659 Language mapping in tumor patients. *Neuroimage* 103, 462–475.
660 <https://doi.org/10.1016/j.neuroimage.2014.08.029>
- 661 Langs, G., Wang, D., Golland, P., Mueller, S., Pan, R., Sabuncu, M.R., Sun, W., Li, K., Liu,
662 H., 2016. Identifying Shared Brain Networks in Individuals by Decoupling Functional
663 and Anatomical Variability. *Cereb. Cortex* 26, 4004–4014.
664 <https://doi.org/10.1093/cercor/bhv189>
- 665 Lin, L.I., 2016. A Concordance Correlation Coefficient to Evaluate Reproducibility Author (s
666): Lawrence I-Kuei Lin Published by : International Biometric Society Stable URL :
667 <http://www.jstor.org/stable/2532051> REFERENCES Linked references are available on
668 JSTOR for thi 45, 255–268.
- 669 Lohmann, G., Ovadia-Caro, S., Jungehülsing, G.J., Margulies, D.S., Villringer, A., Turner,
670 R., 2012. Connectivity concordance mapping: a new tool for model-free analysis of

- 671 FMRI data of the human brain. *Front. Syst. Neurosci.* 6, 13.
672 <https://doi.org/10.3389/fnsys.2012.00013>
- 673 Lyden, P., 2017. Using the National Institutes of Health Stroke Scale. *Stroke* 48, 513–519.
674 <https://doi.org/10.1161/STROKEAHA.116.015434>
- 675 Margulies, D.S., Ghosh, S.S., Goulas, A., Falkiewicz, M., Huntenburg, J.M., Langs, G.,
676 Bezgin, G., Eickhoff, S.B., Castellanos, F.X., Petrides, M., Jefferies, E., Smallwood, J.,
677 2016. Situating the default-mode network along a principal gradient of macroscale
678 cortical organization. *Proc. Natl. Acad. Sci. U. S. A.* 113, 12574–12579.
679 <https://doi.org/10.1073/pnas.1608282113>
- 680 Markov, N.T., Ercsey-Ravasz, M.M., Ribeiro Gomes, A.R., Lamy, C., Magrou, L., Vezoli, J.,
681 Misery, P., Falchier, A., Quilodran, R., Gariel, M.A., Sallet, J., Gamanut, R., Huissoud,
682 C., Clavagnier, S., Giroud, P., Sappey-Marinier, D., Barone, P., Dehay, C., Toroczkai,
683 Z., Knoblauch, K., Van Essen, D.C., Kennedy, H., 2014. A Weighted and Directed
684 Interareal Connectivity Matrix for Macaque Cerebral Cortex. *Cereb. Cortex* 24, 17–36.
685 <https://doi.org/10.1093/cercor/bhs270>
- 686 Nomura, E.M., Gratton, C., Visser, R.M., Kayser, A., Perez, F., D’Esposito, M., 2010. Double
687 dissociation of two cognitive control networks in patients with focal brain lesions. *Proc.*
688 *Natl. Acad. Sci. U. S. A.* 107, 12017–22. <https://doi.org/10.1073/pnas.1002431107>
- 689 Ovadia-Caro, S., Margulies, D.S., Villringer, A., 2014. The value of resting-state functional
690 magnetic resonance imaging in stroke. *Stroke* 45, 2818–24.
691 <https://doi.org/10.1161/STROKEAHA.114.003689>
- 692 Ovadia-Caro, S., Villringer, K., Fiebach, J., Jungehulsing, G.J., van der Meer, E., Margulies,
693 D.S., Villringer, A., 2013. Longitudinal effects of lesions on functional networks after
694 stroke. *J. Cereb. Blood Flow Metab.* 33, 1279–85. <https://doi.org/10.1038/jcbfm.2013.80>
- 695 Park, C., Chang, W.H., Ohn, S.H., Kim, S.T., Bang, O.Y., Pascual-Leone, A., Kim, Y.-H.,
696 2011. Longitudinal changes of resting-state functional connectivity during motor
697 recovery after stroke. *Stroke* 42, 1357–62.
698 <https://doi.org/10.1161/STROKEAHA.110.596155>
- 699 Ramsey, L.E., Siegel, J.S., Baldassarre, A., Metcalf, N. V., Zinn, K., Shulman, G.L., Corbetta,
700 M., 2016. Normalization of network connectivity in hemispatial neglect recovery. *Ann.*
701 *Neurol.* 80, 127–141. <https://doi.org/10.1002/ana.24690>
- 702 Roche, A., 2011. A four-dimensional registration algorithm with application to joint
703 correction of motion and slice timing in fMRI. *IEEE Trans. Med. Imaging* 30, 1546–
704 1554. <https://doi.org/10.1109/TMI.2011.2131152>

- 705 Sacco, R.L., Kasner, S.E., Broderick, J.P., Caplan, L.R., Connors, J.J., Culebras, A., Elkind,
706 M.S.V., George, M.G., Hamdan, A.D., Higashida, R.T., Hoh, B.L., Janis, L.S., Kase,
707 C.S., Kleindorfer, D.O., Lee, J.M., Moseley, M.E., Peterson, E.D., Turan, T.N.,
708 Valderrama, A.L., Vinters, H. V., 2013. An updated definition of stroke for the 21st
709 century: A statement for healthcare professionals from the American heart
710 association/American stroke association. *Stroke* 44, 2064–2089.
711 <https://doi.org/10.1161/STR.0b013e318296aeeca>
- 712 Siegel, J.S., Ramsey, L.E., Snyder, A.Z., Metcalf, N. V., Chacko, R. V., Weinberger, K.,
713 Baldassarre, A., Hacker, C.D., Shulman, G.L., Corbetta, M., 2016. Disruptions of
714 network connectivity predict impairment in multiple behavioral domains after stroke.
715 *Proc. Natl. Acad. Sci.* 113, E4367–E4376. <https://doi.org/10.1073/pnas.1521083113>
- 716 Siegel, J.S., Snyder, A.Z., Ramsey, L., Shulman, G.L., Corbetta, M., 2016. The effects of
717 hemodynamic lag on functional connectivity and behavior after stroke. *J. Cereb. Blood
718 Flow Metab.* 36, 2162–2176. <https://doi.org/10.1177/0271678X15614846>
- 719 Sporns, O., Tononi, G., Kötter, R., 2005. The human connectome: A structural description of
720 the human brain. *PLoS Comput. Biol.* 1, e42.
721 <https://doi.org/10.1371/journal.pcbi.0010042>
- 722 Thomas Yeo, B.T., Krienen, F.M., Sepulcre, J., Sabuncu, M.R., Lashkari, D., Hollinshead,
723 M., Roffman, J.L., Smoller, J.W., Zollei, L., Polimeni, J.R., Fischl, B., Liu, H., Buckner,
724 R.L., 2011. The organization of the human cerebral cortex estimated by intrinsic
725 functional connectivity. *J. Neurophysiol.* 106, 1125–1165.
726 <https://doi.org/10.1152/jn.00338.2011>
- 727 van Dellen, E., Hillebrand, A., Douw, L., Heimans, J.J., Reijneveld, J.C., Stam, C.J., 2013.
728 Local polymorphic delta activity in cortical lesions causes global decreases in functional
729 connectivity. *Neuroimage* 83, 524–532.
730 <https://doi.org/10.1016/j.neuroimage.2013.06.009>
- 731 van den Heuvel, M.P., Sporns, O., 2013. Network hubs in the human brain. *Trends Cogn. Sci.*
732 17, 683–696. <https://doi.org/10.1016/j.tics.2013.09.012>
- 733 van Meer, M.P. a, van der Marel, K., Wang, K., Otte, W.M., El Bouazati, S., Roeling, T. a P.,
734 Viergever, M. a, Berkelbach van der Sprekkel, J.W., Dijkhuizen, R.M., 2010. Recovery
735 of sensorimotor function after experimental stroke correlates with restoration of resting-
736 state interhemispheric functional connectivity. *J. Neurosci.* 30, 3964–72.
737 <https://doi.org/10.1523/JNEUROSCI.5709-09.2010>
- 738 Volz, L.J., Rehme, A.K., Michely, J., Nettekoven, C., Eickhoff, S.B., Fink, G.R., Grefkes, C.,

- 739 2016. Shaping Early Reorganization of Neural Networks Promotes Motor Function after
740 Stroke. *Cereb. Cortex* 26, 2882–2894. <https://doi.org/10.1093/cercor/bhw034>
- 741 Wahlund, L.O., Barkhof, F., Fazekas, F., Bronge, L., Augustin, M., 2001. A New Rating
742 Scale for Age-Related White Matter Changes Applicable to MRI and CT 1318–1323.
- 743 Wang, L., Yu, C., Chen, H., Qin, W., He, Y., Fan, F., Zhang, Y., Wang, M., Li, K., Zang, Y.,
744 Woodward, T.S., Zhu, C., 2010. Dynamic functional reorganization of the motor
745 execution network after stroke. *Brain* 133, 1224–38.
746 <https://doi.org/10.1093/brain/awq043>
- 747 Ward, N.S., 2005. Plasticity and the functional reorganization of the human brain. *Int. J.*
748 *Psychophysiol.* 58, 158–61. <https://doi.org/10.1016/j.ijpsycho.2005.02.009>
- 749 Warren, J.E., Crinion, J.T., Lambon Ralph, M. a, Wise, R.J.S., 2009. Anterior temporal lobe
750 connectivity correlates with functional outcome after aphasic stroke. *Brain* 132, 3428–
751 42. <https://doi.org/10.1093/brain/awp270>
- 752 Woolrich, M.W., Jbabdi, S., Patenaude, B., Chappell, M., Makni, S., Behrens, T., Beckmann,
753 C., Jenkinson, M., Smith, S.M., 2009. Bayesian analysis of neuroimaging data in FSL.
754 *Neuroimage* 45, S173–S186. <https://doi.org/10.1016/j.neuroimage.2008.10.055>
- 755 Young, M.P., Hilgetag, C.-C., Scannell, J.W., 2000. On imputing function to structure from
756 the behavioural effects of brain lesions. *Philos. Trans. R. Soc. B Biol. Sci.* 355, 147–161.
757 <https://doi.org/10.1098/rstb.2000.0555>
- 758 Yushkevich, P.A., Piven, J., Hazlett, H.C., Smith, R.G., Ho, S., Gee, J.C., Gerig, G., 2006.
759 User-guided 3D active contour segmentation of anatomical structures: Significantly
760 improved efficiency and reliability. *Neuroimage* 31, 1116–1128.
761 <https://doi.org/10.1016/j.neuroimage.2006.01.015>
- 762